Spacecraft Angular Velocity Estimation Using Sequential Observations of a Single Directional Vector

Yaakov Oshman*
Technion—Israel Institute of Technology, 32000 Haifa, Israel
and
François Dellus†
Israel Aircraft Industries, Ltd., 56100 Yehud, Israel

A new approach is presented for estimating the angular rate of a tumbling, momentum wheel-equipped spacecraft from sequential measurements of a single directional vector. The wheel's momentum is assumed to be known. The method comprises two stages, a deterministic algorithm that provides a coarse angular velocity estimate and an extended Kalman filter that is initialized using the first-stage crude estimate. This initialization renders the filter accurate and robust. A simulation study is used to demonstrate the method's performance for angular rates of up to 0.5 rad/s. This study shows that the deterministic algorithm can yield angular velocity estimates with bounded reconstruction errors on the order of 1 deg/s, whereas the extended Kalman filter's estimates are accurate, under nominal conditions, to within 0.05 deg/s. The sensitivity of the algorithms to inertia uncertainty of up to 10% of the nominal value is assessed via a simulation study.

Nomenclature

A	=	matrix whose entries are α_i, β_i, γ_i, where i is 1, 2, 3
d/dt	=	total temporal derivative
H	=	spacecraft total angular momentum vector, $N \cdot m \cdot s$
h	=	reaction wheel momentum vector, $N \cdot m \cdot s$
I	=	spacecraft inertia matrix, $kg \cdot m^2$
P	=	extended Kalman filter estimation error covariance matrix
Q	=	process noise covariance
r_i	=	row vectors of A, where i is 1, 2, 3
S	=	directional (sun) unit vector
$\bar{u}, u, \underline{u}$	=	left singular vectors of A
$v, v, \underline{v}$	=	right singular vectors of A
v_s	=	measurement noise vector
w	=	process noise vector
y	=	measured sun vector
$\alpha_i, \beta_i, \gamma_i$	=	coefficients of angular rate quadratic equations, where $i = 1, 2, 3$
β	=	spatial angle between sun vector and spacecraft angular momentum, deg
$\partial/\partial t$	=	local temporal derivative
$\zeta, \zeta, \underline{\zeta}$	=	singular values of A
η_s	=	process noise corresponding to sun vector
η_T	=	process noise corresponding to angular velocity
σ_s^2	=	process noise intensity corresponding to sun vector
σ_T^2	=	process noise intensity corresponding to angular velocity
σ_v^2	=	measurement noise covariance
Ω	=	spacecraft angular velocity vector, rad/s or deg/s
$\cdot$	=	temporal derivative of any symbol

Introduction

IN most practical implementations of attitude control systems on gyro-based spacecraft, attitude rate information is obtained from an onboard triad of rate gyroscopes. This rate information is used in the spacecraft despin, rate damping and control systems, and in the propagation stage of its attitude estimator.[1,2]

Current technology rate gyros are characterized by their low reliability, manifested by a high failure occurrence, as has recently been evidenced by the Hubble Space Telescope, which was put into safe-hold mode on 13 November 1999, after four of its six gyros malfunctioned. Coupled with known cases of unexpected outbursts in satellite thrusters, which often result in hazardous, tumbling situations, these factors motivate the research for the development of alternative rate estimation algorithms. In recent years, the method of attitude determination from vector observations has been extended by several researchers to address the estimation of attitude rate as well, thus facilitating its use on gyroless spacecraft. Gyroless attitude and attitude-rate estimation is, obviously, of prime importance in small, inexpensive, spacecraft, such as the solar, anomalous, magnetospheric particle explorer (SAMPEX), that do not carry gyroscopes but that, nevertheless, need to determine their angular velocity for attitude control and attitude propagation purposes.[3] However, even spacecraft that were designed to carry gyroscopes can benefit from the use of attitude-rate estimation in the event of an unexpected gyro failure,[4] or when the gyros are saturated by high angular rate of the spacecraft.

Most of the existing rate estimation algorithms are based on simultaneous observation of at least two noncollinear vectors and assume or estimate, either explicitly or implicitly, full three-axis attitude knowledge. In Ref. 5, high-bandwidth star-tracker measurements are used solely to drive an error-state extended Kalman filter (EKF), which estimates both the spacecraft attitude quaternion and its angular rate. Reference 6 presents a method for the estimation of spacecraft attitude and angular rate from three-axis magnetometer readings. The method is based on the knowledge of Earth's magnetic field model and takes an orbit to converge. The accuracy obtained is coarse, and the authors suggest that the method be used in emergency modes. Reference 7 presents an essentially deterministic nonlinear estimator for spacecraft angular velocity from measurements of at least two vectors (e.g., sun direction and Earth's magnetic field flux density vector) and their body-referenced time derivatives. The angular velocity is estimated via a least-squares procedure based solely on the angular velocity's kinematics equation and the assumption that, over the time interval between updates, the measured vectors are fixed in inertial space. Reference 8 proposes

a two-stage estimator in which a deterministic batch algorithm that provides a coarse estimate of the angular rate from magnetometer measurements during one satellite orbit is used to initialize a Kalman filter that estimates the orientation and, as a by-product, the angular rate of the spacecraft. Temporal derivatives of Earth's magnetic field measurements are utilized, and the angular velocity estimates are dynamically propagated using Euler's nonlinear equations. The method is designed to work only in the steady-state operational mode of the spacecraft and when the angle between the satellite momentum and Earth's magnetic field is larger than 15 deg. A similar concept assuming explicit knowledge of the spacecraft attitude is presented in Refs. 9 and 10. In Ref. 11, predictive filtering was applied to estimate the attitude quaternion in a gyroless setting. By the use of Euler's equations (assuming that the spacecraft dynamic model is accurately known), the attitude rate was estimated as a by-product from the estimated spacecraft angular momentum. Reference 12 introduces an angular rate estimator (assuming a known attitude), proposing to alleviate the computational complexity normally associated with the nonlinear Euler equations-based EKF by extending the suboptimal interlaced Kalman filter scheme proposed in Ref. 13. This algorithm is able to estimate angular rates from two measured directional vectors and from a single vector for the relatively short durations of eclipses. Another unusual method that attempts to maintain linearity by using the state-dependent Riccati equation is proposed in Ref. 14. Although both Refs. 12 and 14 implicitly assume attitude knowledge to transform the inertial time derivative of an attitude reference vector into body coordinates, Ref. 15 explicitly uses full attitude estimates to drive an angular-rate estimation algorithm. Reference 16 relates filters that directly use raw vector attitude data to estimate the angular rate (the so-called estimation approach) to methods that compute the rate by differentiating full three-axis attitude estimates (the so-called derivative approach).

With the exception of Ref. 10, all of the methods developed to date are designed for low angular-rate implementations. In severe tumbling situations, when the spacecraft attitude as a function of time is unknown, these methods will not work. Given that in these situations the only directional information can be obtained from sun sensors or magnetometers and, in high-altitude (for example, geosynchronous) orbits, only from sun sensors, this work addresses the problem of estimating the angular rate of a satellite in a tumbling situation, based on sequential measurements of a single direction vector. It is assumed that the satellite possesses an angular momentum wheel that provides a constant and known momentum bias. Contrary to most other methods published to date, no other a priori information, for example, full three-axis attitude information, is assumed to be known. Made up of a combination of two markedly different algorithms (a concept also shared by Refs. 8–10), the new method deals with the estimation problem's inherent nonlinearity in a mixed direct/indirect way. In the first stage, a deterministic (point by point) reconstruction algorithm generates a coarse estimate of the satellite angular rate. This algorithm is based on a combination of the kinematics equation of the apparent motion of the direction vector in the spacecraft body-fixed coordinates with the known dynamics equation of the spacecraft that renders the angular rate reconstructible. That the spacecraft angular momentum is constant in inertial space is used in the process of identifying the true, physical angular rate. No approximation of the nonlinearity is involved, and, being deterministic, this algorithm can not diverge with time. The best coarse rate estimate in the first stage (over that stage's operation interval) is then selected to be used in the second stage for the initialization of an EKF, thus rendering the resulting estimate both highly accurate and robust with respect to initial condition uncertainty. The resulting two-stage algorithm combines the advantages of both of its components: the deterministic algorithm allows a coarse estimation of the rate without any a priori knowledge of the spacecraft attitude or attitude rate, and, given the initial estimate of the first stage, the EKF allows for an accurate and fast estimate of the rate.

The remainder of this paper is organized as follows. The mathematical model used to develop the rate estimator is formulated in the next section. The new deterministic, point-by-point angular-rate reconstruction algorithm is then introduced, and two methods are

proposed for its implementation. The presentation of the deterministic algorithm is followed by a discussion of the second stage of the combined rate estimator that consists of an EKF. A numerical simulation study that demonstrates the performance of the new method is presented next. Conclusions are offered in the final section.

Mathematical Model

To enable an analysis of the principal factors affecting the proposed estimation method, an idealized mathematical model of the spacecraft is assumed in this work. Thus, the spacecraft is assumed to obey rigid-body equations of motion, and no energy damping mechanisms are considered. Note, though, that the treatment of a more complex mathematical model (as long as it is known) will not change the general nature of the results obtained herein.

The spacecraft model used in this work corresponds to a geosynchronous satellite with one momentum bias wheel on its Y axis, equipped with coarse sun sensors (CSS). It is assumed that the CSS are located all around the satellite, so that they can provide accurate, high-bandwidth measurements of the sun direction independently of the satellite time-varying attitude. The satellite is assumed to be in a severe tumbling motion, so that the CSS are its only functioning attitude sensors. Because no external torques are acting on the spacecraft, its angular momentum vector is constant in inertial space. The axes of the spacecraft body-fixed coordinate system are set to coincide with the body principal axes. Thus, the spacecraft moment of inertia matrix is

$$I = \text{diag}\{I_{xx}, I_{yy}, I_{zz}\} \qquad (1)$$

The total angular momentum of the satellite is

$$H = I\Omega + h \qquad (2)$$

where $\Omega = [\Omega_x, \Omega_y, \Omega_z]^T$ is the angular velocity and h is the (known) angular momentum of the wheel. From the Euler equation of the spacecraft we have

$$\frac{\partial}{\partial t}\Omega = -I^{-1}(\Omega \times H) \qquad (3)$$

The kinematics equation describing the apparent motion of the observed directional vector in the body-fixed coordinate system is

$$\frac{\text{d}}{\text{d}t}S = \frac{\partial}{\partial t}S + \Omega \times S \qquad (4)$$

where $S = [S_x, S_y, S_z]^T$ is the observed directional unit vector, $(\text{d}/\text{d}t)S$ is the total temporal derivative of S, and $(\partial/\partial t)S$ is the local derivative of S in the spacecraft body-fixed coordinate system.

If the satellite motion in its orbit relative to the sun is negligible during the relevant time period, Eq. (4) yields

$$\frac{\partial}{\partial t}S = -\Omega \times S \qquad (5)$$

Clearly, Eq. (5) shows that the relation between the satellite angular velocity and the sun direction is nonlinear, time-varying, and noninvertible, that is, Ω cannot be computed explicitly from the sun direction vector S and its local derivative $(\partial/\partial t)S$.

Deterministic Algorithm

The idea underlying the development of the deterministic algorithm is that the spacecraft dynamics equation can be used in conjunction with the observed vector's kinematic equation to render the spacecraft angular rate observable. Thus, differentiating Eq. (4), using Eqs. (2) and (3), and remembering that $(\text{d}/\text{d}t)S = 0$ yields

$$\frac{\partial^2 S}{\partial t^2} - I^{-1}[\Omega \times (I\Omega + h)] \times S - \Omega \times (\Omega \times S) = 0 \qquad (6)$$

If the observed directional vector S and its temporal derivatives are known in the body-fixed coordinate system, Eq. (6) constitutes a nonlinear equation for the components of the angular rate vector Ω. To solve this equation, we now proceed as follows.

By the use of Eq. (5), any component of $\boldsymbol{\Omega}$ can be expressed as a function of the other two components and the temporal derivative of $\boldsymbol{S}$. Thus, for example,

$$\Omega_y = \frac{\Omega_x S_y + \dot{S}_z}{S_x} \tag{7a}$$

$$\Omega_z = \frac{\Omega_x S_z - \dot{S}_y}{S_x} \tag{7b}$$

Using Eqs. (7) in the three scalar components of Eq. (6) yields three scalar, uncoupled quadratic equations for the unknown rate component Ω_x:

$$\alpha_1 \Omega_x^2 + \beta_1 \Omega_x + \gamma_1 = 0 \tag{8a}$$

$$\alpha_2 \Omega_x^2 + \beta_2 \Omega_x + \gamma_2 = 0 \tag{8b}$$

$$\alpha_3 \Omega_x^2 + \beta_3 \Omega_x + \gamma_3 = 0 \tag{8c}$$

The coefficients of the quadratic equations (8), listed in the Appendix, are all computable in terms of the observed directional vector, its temporal derivatives, and the known spacecraft dynamic model parameters. Notice that, whereas in the ideal, noiseless case, any of these three scalar equations could be used to solve for the rate component Ω_x, in practice, all three equations are used to alleviate the effects of the measurement noise.

Remark 1: Upon observation of Eqs. (7), it is clear that a singularity condition arises when $S_x \approx 0$. In most typical cases, this singularity is of a temporary nature only (because the spacecraft is subject to a tumbling motion) and can be safely ignored, that is, the solution can be computed for all time points but those for which $S_x = 0$. If, however, this singularity condition persists, alternative sets of equations like Eqs. (7) can be developed, based on the isolation of Ω_y or Ω_z. The resulting sets of equations would have other components of the observed directional vector in their denominators. Thus, in case of singularity in one set of equations, another, nonsingular set of equations can be used.

To solve Eqs. (8) for the angular rate component Ω_x, we first rewrite them in the form

$$A\tilde{\boldsymbol{\Omega}}_x = \boldsymbol{0} \tag{9}$$

where the coefficient matrix is

$$A \triangleq \begin{bmatrix} \alpha_1 & \beta_1 & \gamma_1 \\ \alpha_2 & \beta_2 & \gamma_2 \\ \alpha_3 & \beta_3 & \gamma_3 \end{bmatrix} \tag{10}$$

$$\tilde{\boldsymbol{\Omega}}_x \triangleq \begin{bmatrix} \Omega_x^2 & \Omega_x & 1 \end{bmatrix}^T \tag{11}$$

Because in the ideal, noiseless case, each of the three quadratic equations yields the correct angular rate as one of its solutions, matrix A can be written as

$$A \triangleq \begin{bmatrix} 1 & -(\Omega_{x1} + \Omega_x) & \Omega_{x1}\Omega_x \\ 1 & -(\Omega_{x2} + \Omega_x) & \Omega_{x2}\Omega_x \\ 1 & -(\Omega_{x3} + \Omega_x) & \Omega_{x3}\Omega_x \end{bmatrix} \tag{12}$$

where Ω_{xi}, $i = 1, 2, 3$, are the three spurious solutions corresponding to the three quadratic equations. From Eq. (12), it can be easily established that the rank of A is two. Clearly, then, the solution of Eq. (9) has to satisfy

$$\tilde{\boldsymbol{\Omega}}_x \in \ker A \tag{13}$$

where $\ker A$ denotes the null space of A.

To find the basis vector for $\ker A$, one can proceed with either one of the following two methods.

Singular Value Decomposition Method

Let the singular value decomposition (SVD) of A be

$$A = [\bar{\boldsymbol{u}} \quad \boldsymbol{u} \quad \underline{\boldsymbol{u}}] \begin{bmatrix} \bar{\zeta} & 0 & 0 \\ 0 & \zeta & 0 \\ 0 & 0 & \underline{\zeta} \end{bmatrix} [\bar{\boldsymbol{v}} \quad \boldsymbol{v} \quad \underline{\boldsymbol{v}}]^T \tag{14}$$

where $\bar{\zeta} \geq \zeta \geq \underline{\zeta} \geq 0$ are the singular values of A, and $\{\bar{\boldsymbol{u}}, \boldsymbol{u}, \underline{\boldsymbol{u}}\}$ and $\{\bar{\boldsymbol{v}}, \boldsymbol{v}, \underline{\boldsymbol{v}}\}$ are the corresponding left and right singular vectors, respectively. In the ideal, noiseless case, $\underline{\zeta} = 0$, and the null space of A is readily obtained as

$$\ker A = \operatorname{span}(\underline{\boldsymbol{v}}) \tag{15}$$

In practice, however, $\underline{\zeta} \neq 0$, and the matrix A is of full rank. Because the rank-2 matrix closest to A (in the Frobenius norm sense) is obtained as[17]

$$\tilde{A} = [\bar{\boldsymbol{u}} \quad \boldsymbol{u} \quad \underline{\boldsymbol{u}}] \begin{bmatrix} \bar{\zeta} & 0 & 0 \\ 0 & \zeta & 0 \\ 0 & 0 & 0 \end{bmatrix} [\bar{\boldsymbol{v}} \quad \boldsymbol{v} \quad \underline{\boldsymbol{v}}]^T \tag{16}$$

the null space vector is nevertheless computed using Eq. (15), which then constitutes an optimal approximation of the null space vector.

Vector Product Method

This method uses a result presented by Markley and Mortari in Ref. 18. By the expression of A in terms of its row vectors:

$$A = [\boldsymbol{r}_1 \quad \boldsymbol{r}_2 \quad \boldsymbol{r}_3]^T \tag{17}$$

it can be shown that, in the ideal, noiseless case, each of the vectors

$$\boldsymbol{n}_1 \triangleq \boldsymbol{r}_2 \times \boldsymbol{r}_3, \qquad \boldsymbol{n}_2 \triangleq \boldsymbol{r}_3 \times \boldsymbol{r}_1, \qquad \boldsymbol{n}_3 \triangleq \boldsymbol{r}_1 \times \boldsymbol{r}_2 \tag{18}$$

is parallel to the null space basis vector. In practice, to enhance numerical significance, the solution is chosen as

$$\ker A = \operatorname{span}\left(\arg \max_{n_1,n_2,n_3} \|\boldsymbol{n}\|\right) \tag{19}$$

Remark 2: Note the similarities and differences in underlying assumptions between the deterministic algorithm presented herein and the algorithm presented in Ref. 7. Both methods are based on the measured vector's kinematics equation and the assumption that this vector is essentially fixed in space over the sampling interval. However, unlike Ref. 7, in the method presented herein, only one vector is assumed, and the spacecraft's Euler's equation is fully utilized in the estimation process.

Implementation Issues

Let $[t_0, t_f]$ denote the time interval over which the deterministic reconstruction algorithm is run. This time interval can be regarded as short relative to the spacecraft orbit time. To alleviate the effects of the measurement noise on the reconstructed angular rate and to filter out invalid solutions, the following procedure is used. In the SVD method, a statistical analysis is performed on all smallest singular values at all time points in $[t_0, t_f]$. Time points corresponding to singular values above the 2–σ envelope about the mean singular value are eliminated. Further consistency tests are then performed on the null space basis vectors. These tests reflect the requirements that the first element of these vectors be positive and that the second element (corresponding to the angular velocity component Ω_x) be lower than a given threshold. Finally, all solutions that pass the aforementioned tests are retained, and a time history of the angular velocity in $[t_0, t_f]$ is, thus, obtained. The corresponding time histories of the magnitude of the spacecraft angular momentum vector and the spatial angle between the sun vector and the angular momentum vector are computed. Further consistency tests are then performed to filter out infeasible solutions (outliers). To identify these solutions, the following observations are made.

Because $[t_0, t_f]$ is a short time interval, the sun direction can safely be assumed to be constant throughout it. Also, under the assumption that no external torque acts on the spacecraft, the spacecraft angular momentum vector is constant in inertial space. Hence, during $[t_0, t_f]$, the magnitude of the spacecraft angular momentum and the spatial angle between the sun vector and the spacecraft angular momentum are constant in time:

$$\|\boldsymbol{H}\| = \text{const}, \qquad \forall t \in [t_0, t_f] \qquad (20a)$$

$$\beta = \arccos\left(\frac{\boldsymbol{H} \cdot \boldsymbol{S}}{\|\boldsymbol{H}\|}\right) = \text{const}, \qquad \forall t \in [t_0, t_f] \quad (20b)$$

Obviously, these two conditions are independent of the coordinate system in which they are computed. Now, using the time histories of $\|\boldsymbol{H}\|$ and β over $[t_0, t_f]$, infeasible solutions are defined as those that violate the conditions expressed in Eqs. (20). These infeasible solutions are identified and eliminated, leaving a batch of feasible reconstructed angular rates over the interval $[t_0, t_f]$.

Stationary Motion

Stationary motion conditions occur when both the angular velocity and sun vectors are constant in time, as measured in the body-fixed coordinate system. In these special cases, the reconstruction of the angular velocity becomes much easier.

Substituting $(\partial/\partial t)\boldsymbol{\Omega} = \boldsymbol{0}$ and $(\partial/\partial t)\boldsymbol{S} = \boldsymbol{0}$ into Eqs. (3) and (5), respectively, yields

$$\boldsymbol{\Omega} \times \boldsymbol{H} = \boldsymbol{0} \qquad (21a)$$

$$\boldsymbol{\Omega} \times \boldsymbol{S} = \boldsymbol{0} \qquad (21b)$$

which means that the vectors $\boldsymbol{\Omega}$, $\boldsymbol{H}$, and $\boldsymbol{S}$ are collinear. Using Eq. (2) in Eq. (21a) yields

$$\boldsymbol{\Omega} \times (I\boldsymbol{\Omega}) = -\boldsymbol{\Omega} \times \boldsymbol{h} \qquad (22)$$

which forms the geometrical basis for the reconstruction of the angular velocity vector in stationary motion cases.

Using Eqs. (21b) and (22) in the same manner as was done in the development of Eqs. (8) yields the following two stationary motion solutions.

Case 1

The sun direction and the wheel angular momentum vectors satisfy the relation

$$S_y = \frac{S_z h_y S_x (I_{xx} - I_{zz})}{(I_{xx} - I_{yy})h_z S_x + (I_{yy} - I_{zz})h_x S_z} \qquad (23)$$

In this case, the angular velocity vector is

$$\Omega_x = -\frac{h_x S_z - h_z S_x}{(I_{xx} - I_{zz})S_z} \qquad (24a)$$

$$\Omega_y = -\frac{h_y(h_x S_z - h_z S_x)}{(I_{xx} - I_{yy})h_z S_x + (I_{yy} - I_{zz})h_x S_z} \qquad (24b)$$

$$\Omega_z = -\frac{h_x S_z - h_z S_x}{(I_{xx} - I_{zz})S_x} \qquad (24c)$$

Case 2

The sun direction and the wheel angular momentum vectors satisfy the relation

$$S_z = \frac{S_y h_z S_x (I_{xx} - I_{yy})}{(I_{xx} - I_{zz})h_y S_x + (I_{zz} - I_{yy})h_x S_y} \qquad (25)$$

In this case, the angular velocity vector is

$$\Omega_x = \frac{h_y S_x - h_x S_y}{(I_{xx} - I_{yy})S_y} \qquad (26a)$$

$$\Omega_y = \frac{h_y S_x - h_x S_y}{(I_{xx} - I_{yy})S_x} \qquad (26b)$$

$$\Omega_z = -\frac{h_z(h_y S_x - h_x S_y)}{(I_{xx} - I_{zz})h_y S_x + (I_{zz} - I_{yy})h_x S_y} \qquad (26c)$$

Unobservable Stationary Motion

As noted earlier, in stationary motion the vectors $\boldsymbol{\Omega}$, $\boldsymbol{H}$, and $\boldsymbol{S}$ are collinear. When these vectors are also collinear with the momentum wheel's angular momentum vector, a singular, unobservable situation arises because Eq. (22) then yields

$$\boldsymbol{\Omega} \times (I\boldsymbol{\Omega}) = \boldsymbol{0} \qquad (27)$$

To identify the situations where this condition occurs, Eq. (27) is rewritten as

$$\Omega_y \Omega_z (I_{zz} - I_{yy}) = 0 \qquad (28a)$$

$$\Omega_x \Omega_z (I_{zz} - I_{xx}) = 0 \qquad (28b)$$

$$\Omega_x \Omega_y (I_{yy} - I_{xx}) = 0 \qquad (28c)$$

From Eqs. (28), the following three possible singular situations are identified. The first singular case is where all principal moments of inertia are identical, a rare case termed in the sequel as "spherical spacecraft." Notice that, in this case, a singularity arises in Eqs. (24) and (26). The second case is where only two of the principal moments of inertia are equal. In this case, the angular velocity must lie in the plane spanned by the axes corresponding to the two identical moments of inertia, or in the plane orthogonal to it, that is, along the third principal axis. The third case is where all moments of inertia are different. In this case, the angular velocity must lie along one of the principal axes.

From Eqs. (24) and (26), it might seem that additional singular cases exist when either S_y or S_z vanish. However, it is easy to show that these cases are actually manifestations of conditions (28). Suppose, for example, that $S_z = 0$. From Eq. (23), it follows that $S_y = 0$, rendering

$$\boldsymbol{S} = [1 \quad 0 \quad 0]^T \qquad (29)$$

Because, in stationary motion, $\boldsymbol{\Omega}$ and $\boldsymbol{S}$ are collinear, it follows that $\boldsymbol{\Omega}$ is expressible as

$$\boldsymbol{\Omega} = [\Omega_x \quad 0 \quad 0]^T \qquad (30)$$

Now, because $\boldsymbol{H}$ is also collinear with $\boldsymbol{\Omega}$ in stationary motion, it follows from Eq. (2) that the wheel's momentum vector must also be collinear with $\boldsymbol{\Omega}$, which leads to Eq. (27) as discussed earlier. It is easy to verify that $S_y = 0$ renders exactly the same result.

From the preceding discussion, it can be concluded that only one unobservable stationary motion case exists, when the vectors $\boldsymbol{\Omega}$, $\boldsymbol{H}$, $\boldsymbol{S}$, and $\boldsymbol{h}$ are collinear. Fortunately, this situation is easy to detect and, hence, to avoid, by stirring the spacecraft out of it via commanding an appropriate attitude change using the spacecraft attitude control system.

EKF

The EKF provides a filtered solution of the angular velocity, statistically taking into account the measurement noise, which was not optimally filtered in the deterministic solution. The algorithm is initialized using the coarse deterministic solution, which greatly enhances its convergence and robustness with respect to initial state uncertainty.

The state vector is defined as

$$\boldsymbol{x} \stackrel{\triangle}{=} \begin{bmatrix} \boldsymbol{S} \\ \boldsymbol{\Omega} \end{bmatrix} \qquad (31)$$

The corresponding state equations are obtained from Eqs. (3) and (5). To compensate for the inaccuracy introduced by the assumption $(\mathrm{d}/\mathrm{d}t)\boldsymbol{S} \approx \boldsymbol{0}$, process noise is added to the state equations of the directional vector components. Also, to compensate for residual and unmodeled torques, process noise is added to the angular rate

state equations. Because of the normalization constraint on the sun direction vector, the process noise vector driving the state equations of the sun vector components must be orthogonal (to first order) to the sun vector. To reflect this constraint, the idempotent orthogonal projector onto the orthogonal complement of span (S) is used to write the process noise vector as

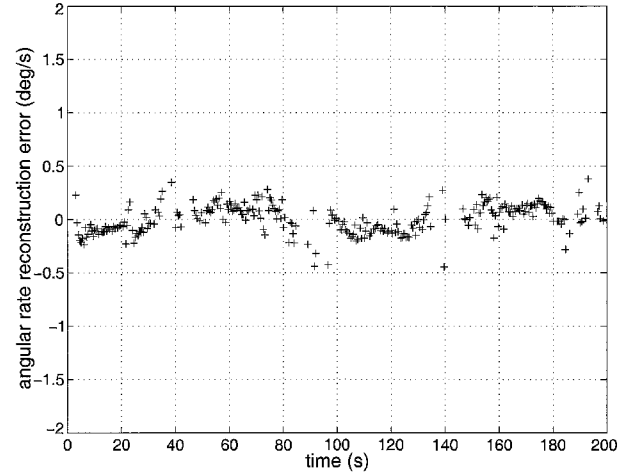$$w = \begin{bmatrix} (I_3 - SS^T)\eta_s \\ I^{-1}\eta_T \end{bmatrix} \qquad (32)$$

where

$$\eta_s = \begin{bmatrix} \eta_{s_x} \\ \eta_{s_y} \\ \eta_{s_z} \end{bmatrix}, \qquad \eta_T = \begin{bmatrix} \eta_{T_x} \\ \eta_{T_y} \\ \eta_{T_z} \end{bmatrix} \qquad (33)$$

are mutually independent zero-mean white-noise vectors distributed as $\eta_s \sim \mathcal{N}[0, \sigma_s^2 I_3 \delta(t)]$ and $\eta_T \sim \mathcal{N}[0, \sigma_T^2 I_3 \delta(t)]$, and I_3 is the three-dimensional identity matrix. The resulting intensity matrix of the process noise w is
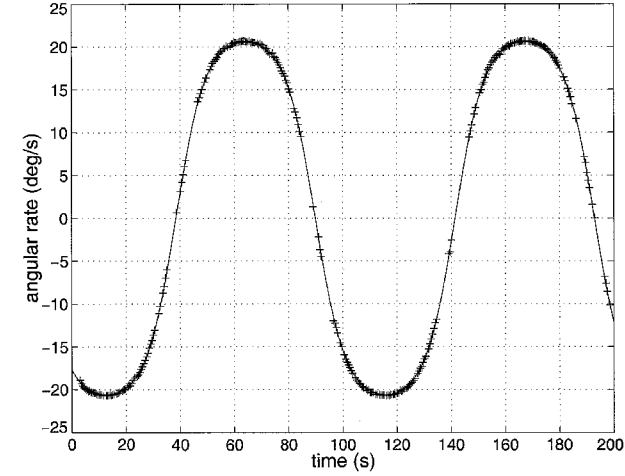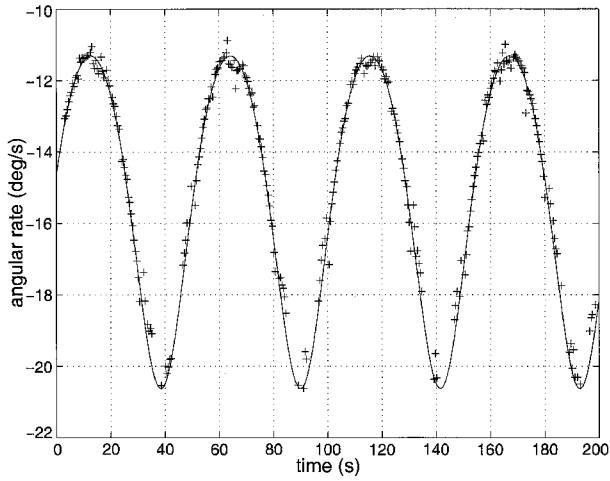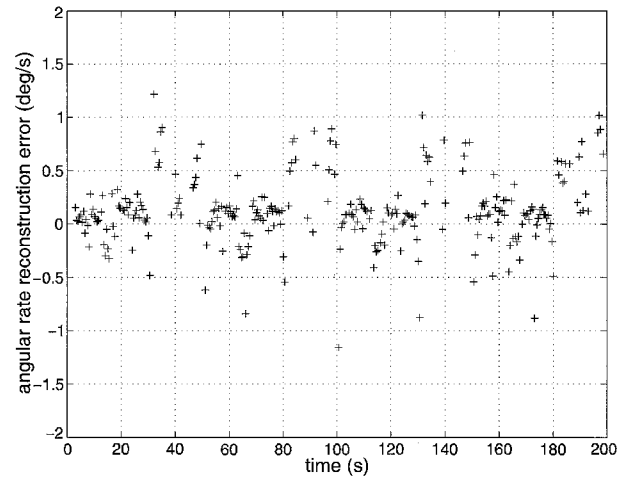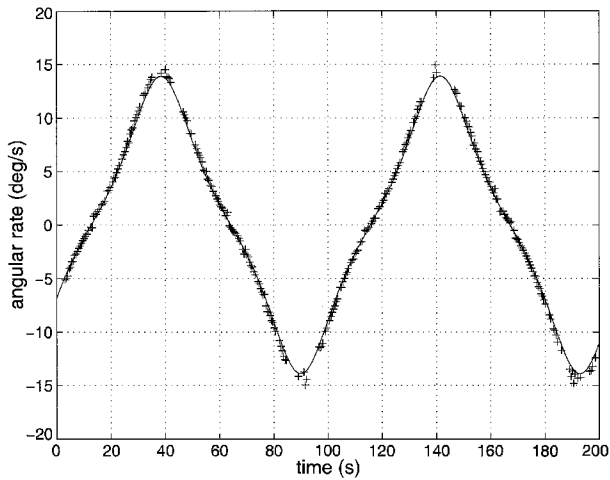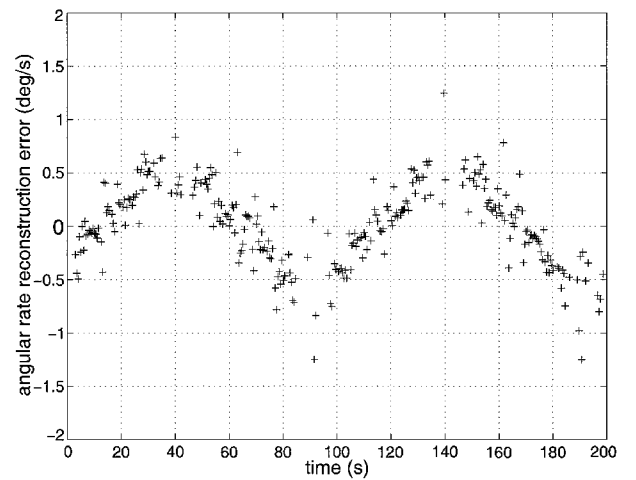
Fig. 1 Angular velocity reconstruction using the deterministic algorithm: ——, true angular rate and +, reconstructed angular rate and rate reconstruction error; a) Ω_x, c) Ω_y, and e) Ω_z: true and reconstructed rates; b) Ω_x, d) Ω_y, and f) Ω_z: rate reconstruction errors.

$$Q = \begin{bmatrix} \left(I_3 - SS^T\right)\sigma_s^2 & \vdots & 0 \\ \hdashline 0 & \vdots & I^{-2}\sigma_T^2 \end{bmatrix} \quad (34)$$

With consideration given again to the normalization constraint on the sun direction vector, the measurement equation is written as

$$y = S + \left(I_3 - SS^T\right)v_s \quad (35)$$

where $v_s \sim \mathcal{N}(0, \sigma_v^2)$.

Notice that the measurement noise covariance matrix, $(I_3 - SS^T)\sigma_v^2$, is singular. However, Shuster[19] used Markley's result in Ref. 20 to show that any axially symmetric probability density on the unit sphere is practically indistinguishable, at any point, from the corresponding density on a plane tangent to that point. Therefore, a nonsingular covariance (obtained by adding a small positive diagonal matrix to the measurement covariance) can be used with no loss in error. The EKF's state vector and dynamic model (including the process and measurement covariance matrices) are initialized using the coarse angular velocity estimate obtained from the deterministic algorithm.

Remark 3: Because the deterministic reconstruction algorithm can be continuously run during the EKF's operation, it can be used to provide an independent, crude, online measure for the performance of the EKF. In particular, the deterministic algorithm can serve to detect possible divergence of the EKF and, should this happen, to allow for a quick reset of the EKF by providing an appropriate initialization for the restarted filter.

Simulation Study

A simulation study was performed to demonstrate the performance of the new estimation method. The inertia matrix of the simulated spacecraft was

$$I = \text{diag}\{600, 400, 700\} \text{ kg} \cdot \text{m}^2 \quad (36)$$

The vector measurement noise was a zero-mean Gaussian process with a standard deviation of $\sigma_v = 0.033$ deg. Each simulation started by running the deterministic algorithm for 200 s, with a sampling interval of 0.5 s. This yielded 400 deterministic estimates over that 200-s interval, which were then scanned to filter out infeasible solutions as explained earlier [using Eqs. (20)]. The EKF algorithm was then initialized by the best deterministic estimate (in a manner described in the sequel) and run for an additional 200 s.

Deterministic Algorithm

Figure 1 shows the true and reconstructed spacecraft angular rates, along with the angular rate reconstruction errors, as obtained using the deterministic algorithm (SVD method) in a single representative run. Note that the vector product method gave very similar results to the SVD method, although the SVD method proved to be slightly more accurate. Therefore, the results presented herein refer to the SVD method only. In practice, the choice between these two methods will be based on additional implementation considerations, such as computational burden and the feasibility of performing SVD onboard the spacecraft computer.

The initial values randomly chosen for this run were

$$h = \begin{bmatrix} 0 & -24.14 & 0 \end{bmatrix}^T \text{ N} \cdot \text{m} \cdot \text{s} \quad (37a)$$

$$\Omega = \begin{bmatrix} -0.3079 & -0.2558 & -0.1188 \end{bmatrix}^T \text{ rad/s} \quad (37b)$$

$$S = \begin{bmatrix} 0.2779 & -0.9313 & 0.2355 \end{bmatrix}^T \quad (37c)$$

As can be seen from Fig. 1, the deterministically reconstructed angular rate components are, in general, unbiased, and the reconstruction error is generally bounded below 1 deg/s. Note that the deterministic solution does not always exist: As explained earlier, a few of the solutions were rejected because they violated the consistency conditions based on the angular momentum vector (constant norm and constant direction).

Figure 2 shows the angular momentum norm and spatial angle reconstruction errors for this run, as obtained using the deterministic
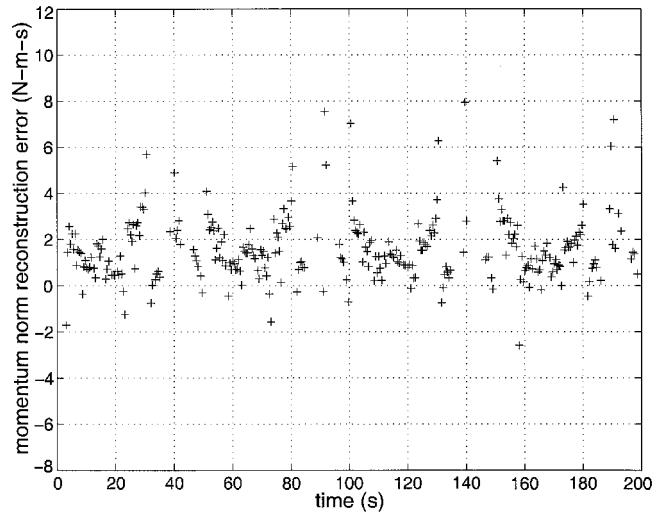
a) **Magnitude**
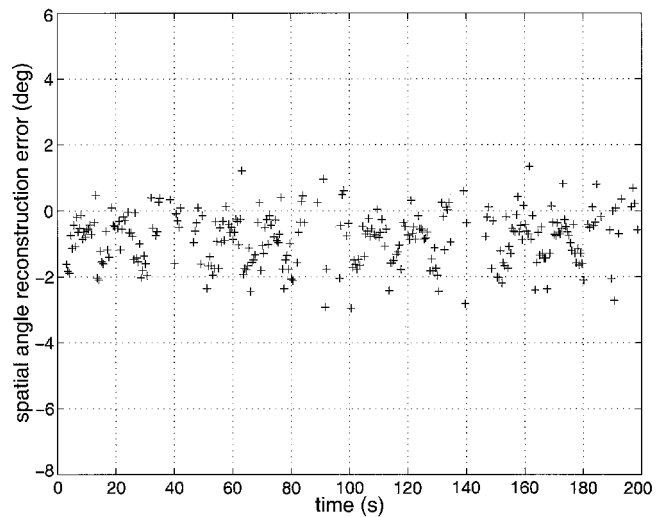
b) **Spatial angle**

Fig. 2   Angular momentum reconstruction error using the deterministic algorithm.

algorithm (SVD method). The true values were 238.82 N $\cdot$ m $\cdot$ s and 78.68 deg, respectively. Figure 2 provides a measure for the quality of the angular rate reconstruction and shows that, although the reconstructed angular momentum (magnitude and direction) is biased, the reconstruction error is relatively small and does not diverge. Thus, the angular momentum magnitude error is smaller than 8 N $\cdot$ m $\cdot$ s and the momentum angle error is smaller than 3 deg throughout the run.

EKF

With the angular velocity reconstructed using the deterministic algorithm in the representative case as discussed earlier, the EKF was then run. The EKF was initialized by the best deterministically reconstructed angular velocity estimate throughout the run. This best estimate was defined as the estimate associated with the closest angular momentum vector estimate (in terms of its magnitude and spatial angle) to the mean of the angular momentum estimates over the entire run. In the case considered, this best estimate was computed at $t = 158.0$ s, and the EKF was then run for an additional 200 s from that point.
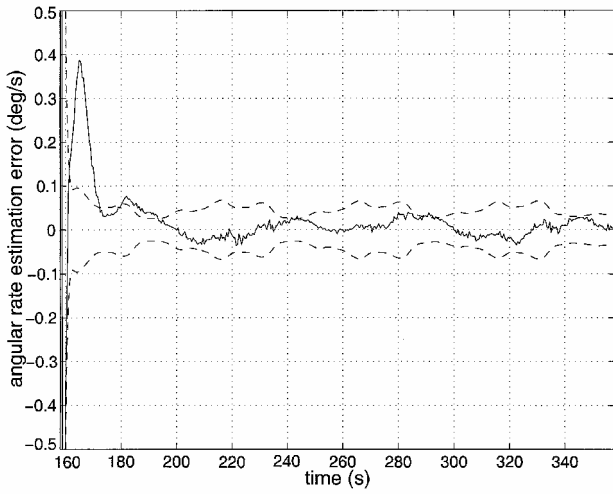
The initial estimation error covariance was

$$P_0 = \text{diag}\{0.01, 0.01, 0.01, 0.2 \text{ rad}^2/\text{s}^2, 0.2 \text{ rad}^2/\text{s}^2, 0.2 \text{ rad}^2/\text{s}^2\}$$
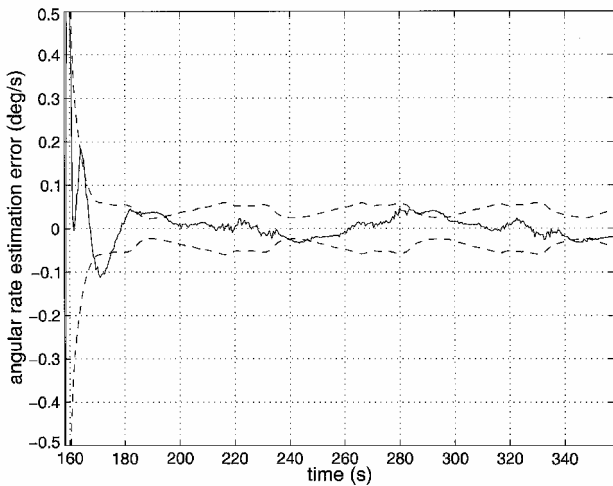
$$(38)$$

State propagation was performed by integrating Euler's equation using the MATLAB® ODE23 integrator. For the process
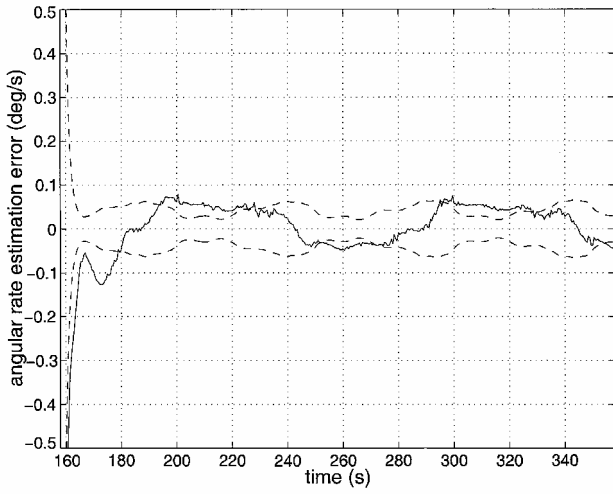
a)

b)

c)

Fig. 3   EKF angular velocity estimation: ——, estimation error and - - -, estimation error 1-σ envelope; a) Ω_x, b) Ω_y, and c) Ω_z.

noise covariance, the following values were used: $\sigma_s^2 = 10^{-5}$ and $\sigma_T^2 = 0.01 \ \text{N}^2 \cdot \text{m}^2$.

Figure 3 shows the angular velocity components estimation errors in this case. As expected, the EKF clearly outperforms the deterministic algorithm. It takes the EKF about 20 s (40 measurements) to converge. The angular rate estimate is unbiased and its 1–σ envelope is generally below about 0.05 deg/s. Remember, however, that the robust performance of the EKF is obtained by using the deterministic algorithm's output as the initial state for the EKF.
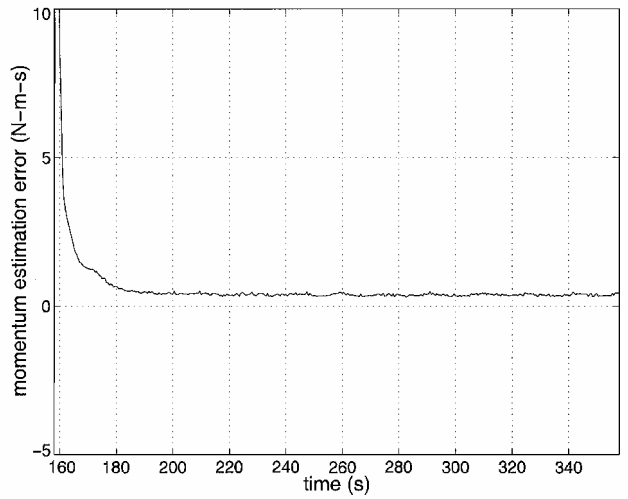

a) Magnitude
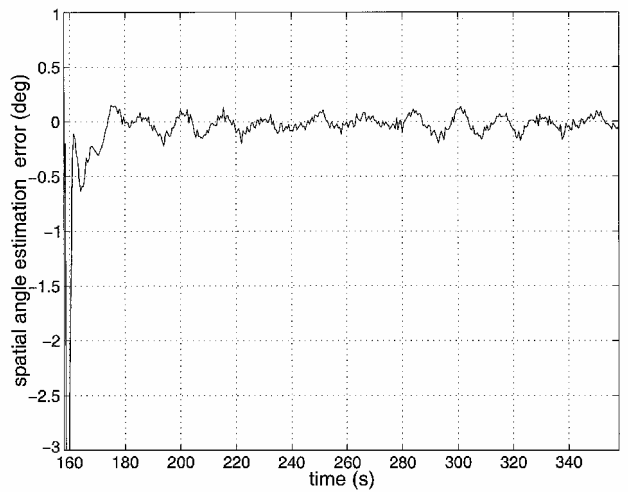
b) Spatial angle

Fig. 4   Angular momentum estimation error using the EKF.

Figure 4 shows the angular momentum norm and spatial angle estimation errors in this case. Recall that these variables are not directly estimated by the EKF but are computed using the estimated attitude rate and filtered sun vector. It can be observed from Fig. 4 that, although the estimate of the momentum magnitude is somewhat biased, the total momentum vector (magnitude and direction) is estimated quite satisfactorily using the EKF's estimate, which renders an indication about that estimate's quality. In particular, the steady-state values of the angular momentum magnitude and direction estimation errors are smaller than 0.5 N $\cdot$ m $\cdot$ s and 0.2 deg, respectively. Comparing these values to the results obtained using the deterministic algorithm demonstrates the superior filtering effect of the EKF.

Monte Carlo Study

A 300-run Monte Carlo simulation study was performed to assess statistically the performance of both the deterministic and the EKF algorithms. In this study, the sun vector observed in the body-fixed coordinate system at the beginning of each simulation run was set by randomly sampling each of its components from a uniform distribution over $[-1, 1]$ and then normalizing the resulting vector to unity norm. The magnitude of the initial angular velocity of the spacecraft was sampled from a uniform distribution over the interval $[0, 0.5]$ rad/s. The direction of the spacecraft initial angular velocity was separately sampled in a manner similar to the sampling of the sun vector. The wheel's angular momentum was along the $-Y$ axis, with a magnitude that was randomly sampled from a uniform distribution over the interval $[20, 30]$ N $\cdot$ m $\cdot$ s.
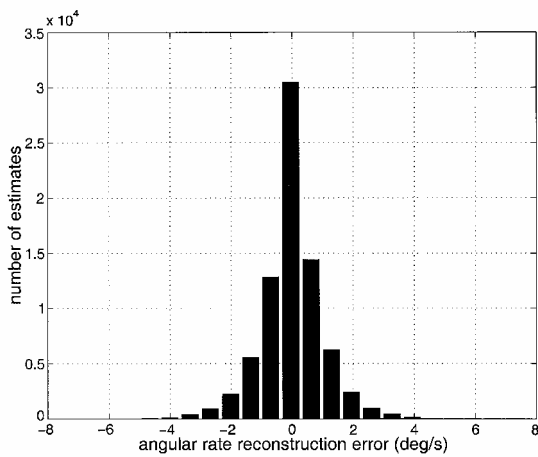
To allow for a better assessment of the statistical nature of the results, estimation error histograms corresponding to the estimated
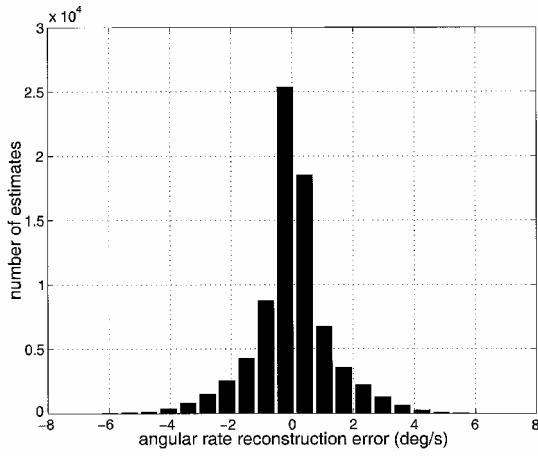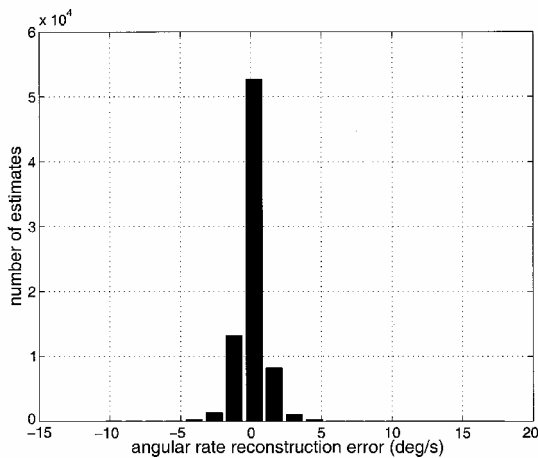
Fig. 5   Histogram of angular velocity reconstruction error using the deterministic algorithm: a) Ω_x, b) Ω_y, and c) Ω_z.
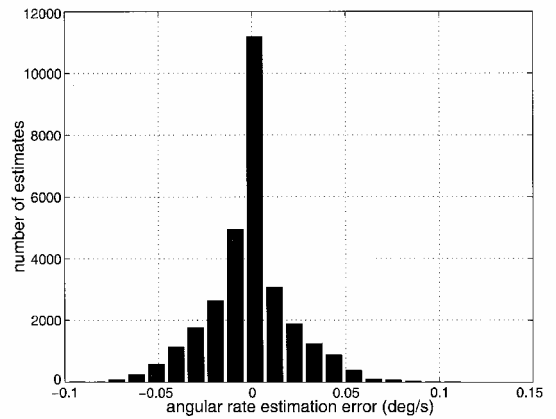
Table 1   Monte Carlo 1-σ estimation errors

Parameter	Deterministic algorithm	EKF
Ω_x, deg/s	1.24	0.022
Ω_y, deg/s	0.98	0.014
Ω_z, deg/s	0.99	0.017
$\|H\|$, N $\cdot$ m $\cdot$ s	5.08	0.154
β, deg	5.10	0.054
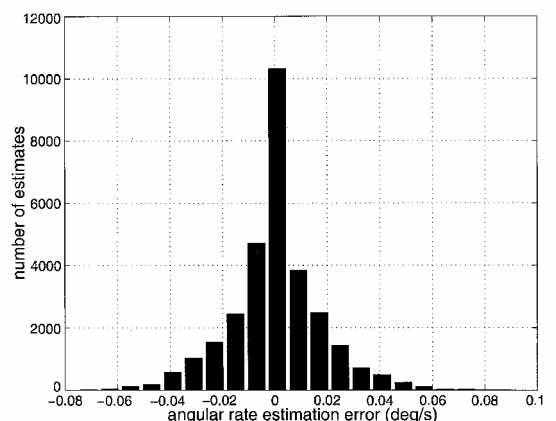
Fig. 6   Histogram of EKF angular velocity estimation error: a) Ω_x, b) Ω_y, and c) Ω_z.

angular-rate components are shown. Figure 5 presents histograms of the deterministic reconstruction errors of the three angular-rate components. The histograms have an approximate symmetric shape, with mode occurring about the zero reconstruction error.

Figure 6 presents histograms of the corresponding rms errors obtained using the EKF algorithm. Again, all histograms display approximate symmetric shape, centered about the zero estimation error.
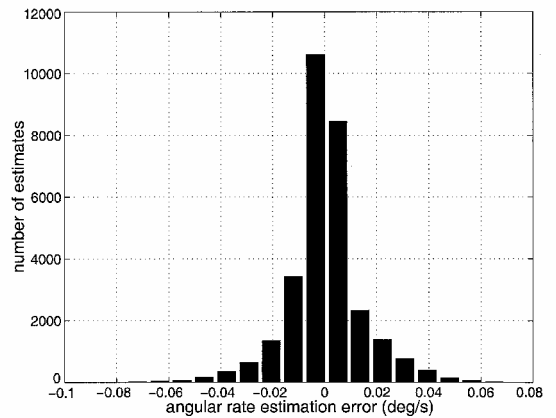
The statistical moments (mean and standard deviation) of these runs are summarized in Table 1. Also shown in Table 1 are the moments of the reconstruction and estimation errors of the momen-

tum vector magnitude and direction, as computed using the corresponding angular velocity estimates. Predictably, the EKF's estimate clearly outperforms the estimate provided by the deterministic algorithm. Nevertheless, even the deterministic algorithm's coarse estimate yields 1-σ errors on the order of just 1 deg/s.

In passing, note again that the mathematical model assumed in this work is somewhat idealized, in that various real-world effects were left out of the simulation. Therefore, though providing a good

check of the proposed algorithm and an indication of the algorithm's viability, the numerical results obtained in the simulation study can not be taken to represent a particular system's real-world performance.

Effects of Model Uncertainty

As noted earlier, the algorithms presented in this paper can be used during initial acquisition (despin), in the stage where the spacecraft is injected into orbit. In this stage, the mathematical model of the spacecraft is generally very well known: The fuel tanks are still full, eliminating the effects of sloshing, and the spacecraft is still at the beginning of its life, rendering its prelaunch, precisely measured dynamic model highly accurate. However, at other stages during the spacecraft's life, some uncertainty in the dynamic model can be expected. To study the effects of this uncertainty, a 300-run Monte Carlo study was performed. In the runs comprising this study, each of the spacecraft's principal moments of inertia was independently sampled from a uniform distribution over a conservative interval of 10% of the nominal moment of inertia, centered about that nominal value. The deterministic algorithm used was identical to that used in the nominal case presented earlier. However, to improve the EKF's capability to cope with the inertia uncertainty, its bandwidth (BW) had to be opened up by increasing the process noise covariance term to $\sigma_T^2 = 5$ N$^2 \cdot$ m^2.

Figure 7 presents histograms of the deterministic reconstruction errors of the three angular rate components in the presence of inertia uncertainty. Note the general similarity of these error histograms to those obtained in the nominal case. Again, the histograms have approximate symmetric shapes, with modes occurring about the zero reconstruction error.

Figure 8 presents histograms of the corresponding rms errors obtained using the high-BW EKF algorithm in the presence of inertia uncertainty. All histograms display approximate symmetric shapes, centered about the zero estimation error, but the errors are significantly larger than those corresponding to the nominal case.

The statistical moments (mean and standard deviation) of these runs are summarized in Table 2. Also shown in Table 2 are the moments of the reconstruction and estimation errors of the momentum vector magnitude and direction, as computed using the corresponding angular velocity estimates. Quite remarkably, the deterministic algorithm's performance degradation due to the inertia uncertainty is hardly noticeable. On the other hand, even though the BW of the EKF was significantly opened up, its performance deteriorated relative to the nominal case by about an order of magnitude (1–σ estimation error of about 0.2 deg/s, as compared with about 0.02 deg/s in the nominal case). Note, though, that even this degraded performance should suffice for most high-dynamics applications.

Finally, a Monte Carlo analysis was performed to assess the performance of the high-BW EKF in the nominal (exact inertia) case. The results of this study are summarized in Table 3. Clearly, this filter performs worse than the filter optimally tuned to the nominal

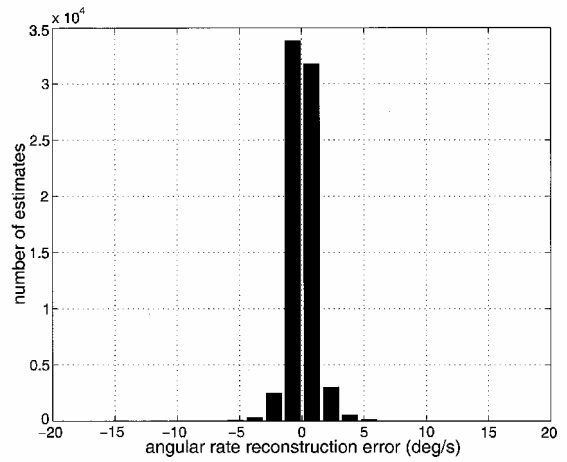Table 2   Monte Carlo 1–σ estimation errors
with inertia uncertainty

Parameter	Deterministic algorithm	High-BW EKF
Ω_x, deg/s	1.26	0.22
Ω_y, deg/s	1.00	0.22
Ω_z, deg/s	1.01	0.20
$\|H\|$, N $\cdot$ m $\cdot$ s	6.58	2.95
β, deg	5.53	1.29

Table 3   Monte Carlo 1–σ
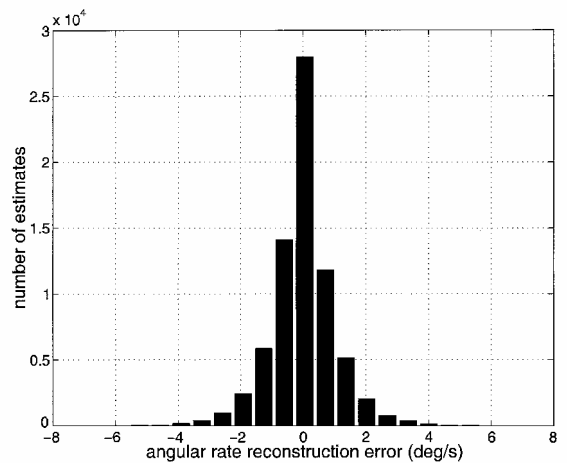estimation errors of high-BW EKF
in nominal (no uncertainty) case

| Parameter	1–σ estimation error
Ω_x, deg/s	0.032
Ω_y, deg/s	0.044
Ω_z, deg/s	0.028
$\|H\|$, N $\cdot$ m $\cdot$ s	0.332
β, deg	0.287
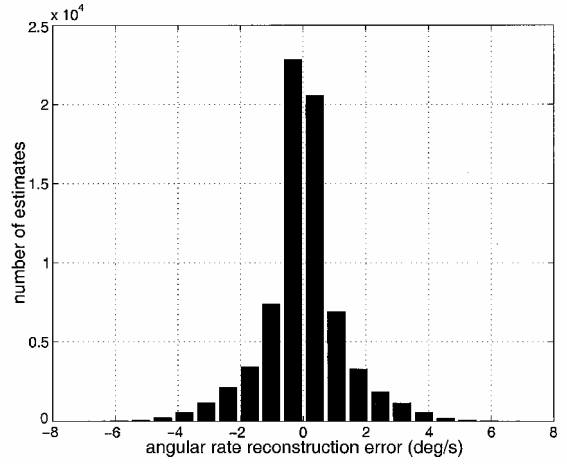
a)

b)

c)

Fig. 7   Histogram of angular velocity reconstruction error using the deterministic algorithm in the presence of inertia uncertainty: a) Ω_x, b) Ω_y, and c) Ω_z.

case, as could be expected. Nevertheless, its performance degradation (with estimation error smaller than 0.05 deg/s) is insignificant in most applications.

The results presented herein show that the EKF algorithm exhibits sensitivity with respect to inertia terms' uncertainty. Although this sensitivity can be effectively accommodated by opening up the BW of the filter, a more rigorous solution would be to estimate the inertia correction terms online (along with the estimation of the angular velocity components), as was done, for example, in Refs. 21 and 22. Another recently proposed method to cope with inertia uncertainty

a)

b)

c)
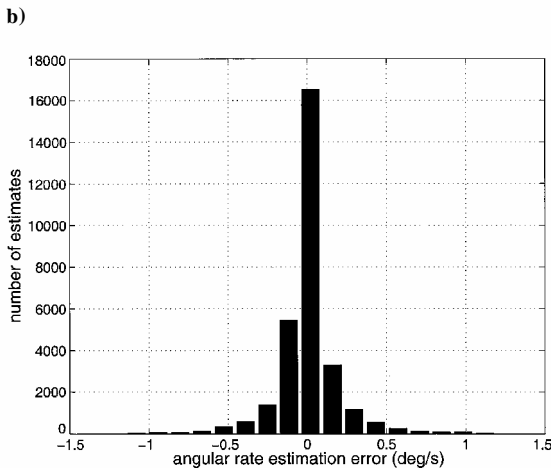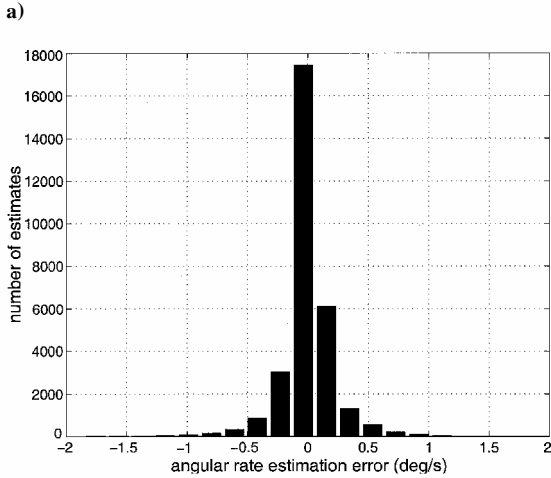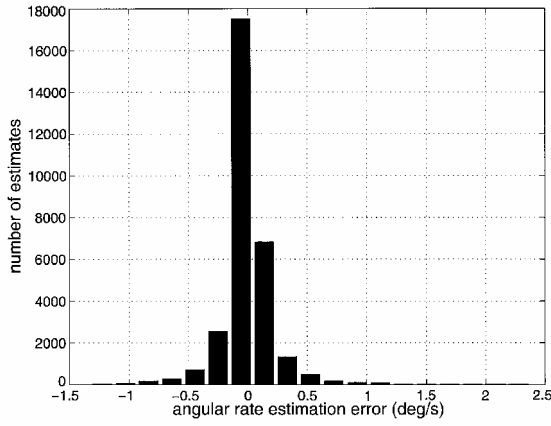
Fig. 8   Histogram of high-BW EKF angular velocity estimation error in the presence of inertia uncertainty: a) Ω_x, b) Ω_y, and c) Ω_z.

is based on statistically testing the EKF's innovations process for whiteness.[23]

Conclusions

A new method was presented for the estimation of the angular rate of a tumbling, momentum wheel-equipped spacecraft from sequential measurements of a single directional vector. No a priori attitude knowledge is assumed, but the dynamic model of the spacecraft and the reaction wheel's momentum are assumed to be known. The method consists of a deterministic (point-by-point) algorithm that provides a coarse estimate of the angular velocity of the spacecraft and an EKF that is initialized using the deterministic estimate. A Monte Carlo simulation study was used to demonstrate the performance of the method for angular rates up to 0.5 rad/s. Given conservatively noisy measurements, the deterministic algo-

rithm yielded bounded 1σ angular rate reconstruction errors on the order of 1 deg/s, whereas the EKF yielded 1σ rate estimation errors on the order of 0.05 deg/s.

The performance of the new method renders it highly useful for estimation of spacecraft body rates in gyroless spacecraft. In addition, the new method can also add important capability to gyro-equipped spacecraft during initial acquisition and/or safe-hold recovery phases.

Appendix: Coefficients of Quadratic Equations (8)

In this Appendix the coefficients of the quadratic equations (8) are listed:

$$\alpha_1 = \frac{\left(I_{xx}I_{yy} - I_{yy}^2\right)S_y^2 + \left(I_{xx}I_{zz} - I_{zz}^2\right)S_z^2}{I_{zz}I_{yy}S_x} \tag{A1a}$$

$$\beta_1 = -\frac{h_y S_y}{I_{zz}} - \frac{h_z S_z}{I_{yy}} + \frac{h_x S_y^2}{I_{zz}S_x} + \frac{h_x S_z^2}{I_{yy}S_x}$$
$$- \frac{(I_{zz} + I_{yy} - I_{xx})I_{yy}S_y\dot{S}_z + (I_{xx} - I_{yy} - I_{zz})I_{zz}S_z\dot{s}_y}{I_{zz}I_{yy}S_x} \tag{A1b}$$

$$\gamma_1 = \frac{h_x S_y \dot{S}_z}{I_{zz}S_x} - \frac{h_x S_z \dot{S}_y}{I_{yy}S_x} - \frac{\left(\dot{S}_y^2 + \dot{S}_z^2\right)I_{yy}I_{zz}}{I_{yy}I_{zz}S_x} - \ddot{S}_x \tag{A1c}$$

$$\alpha_2 = \frac{\left(I_{xx}I_{yy} - I_{xx}^2\right)S_y}{I_{zz}I_{xx}} + \frac{\left(I_{yy}I_{zz} - I_{zz}^2\right)S_y S_z^2}{I_{zz}I_{xx}S_x^2} \tag{A2a}$$

$$\beta_2 = \frac{h_y S_x}{I_{zz}} - \frac{h_x S_y}{I_{zz}} - \frac{(h_z S_y - h_y S_z)S_z}{I_{xx}S_x}$$
$$+ \frac{(I_{yy} + I_{zz} - I_{xx})I_{xx}\dot{S}_z}{I_{zz}I_{xx}} + \frac{(I_{xx} - I_{yy} + I_{zz})I_{zz}S_y S_z\dot{S}_y}{I_{zz}I_{xx}S_x^2}$$
$$+ \frac{(I_{xx} + I_{yy} - I_{zz})I_{zz}S_z^2\dot{S}_z}{I_{zz}I_{xx}S_x^2} \tag{A2b}$$

$$\gamma_2 = -\frac{h_y \dot{S}_z}{I_{zz}} - \frac{S_z \dot{S}_y^2}{S_x^2} - \frac{(h_y \dot{S}_y + h_z \dot{S}_z)I_{zz}S_z}{I_{xx}I_{zz}S_x}$$
$$- \frac{(I_{xx} + I_{yy} - I_{zz})I_{zz}\dot{S}_y\dot{S}_z S_z}{I_{xx}I_{zz}S_x^2} - \ddot{S}_y \tag{A2c}$$

$$\alpha_3 = \frac{(I_{zz} - I_{xx})I_{xx}S_z}{I_{xx}I_{yy}} + \frac{(I_{yy} - I_{zz})I_{yy}S_z S_y^2}{I_{xx}I_{yy}S_x^2} \tag{A3a}$$

$$\beta_3 = \frac{h_z S_x - h_x S_z}{I_{yy}} + \frac{h_z S_y^2 - h_y S_y S_z}{I_{zz}S_x} + \frac{(I_{xx} - I_{yy} - I_{zz})I_{xx}\dot{S}_y}{I_{xx}I_{yy}}$$
$$+ \frac{(I_{zz} - I_{yy} - I_{xx})I_{yy}S_y S_z\dot{S}_z + (I_{yy} - I_{xx} - I_{zz})I_{yy}S_y^2\dot{S}_y}{I_{xx}I_{yy}S_x^2} \tag{A3b}$$

$$\gamma_3 = \frac{h_x \dot{S}_y}{I_{yy}} + \frac{S_z \dot{S}_z^2}{S_x^2} + \frac{(h_y \dot{S}_y + h_z \dot{S}_z)I_{yy}S_y}{I_{xx}I_{yy}S_x}$$
$$+ \frac{(I_{yy} - I_{xx} - I_{zz})I_{yy}\dot{S}_y\dot{S}_z S_y}{I_{xx}I_{yy}S_x^2} - \ddot{S}_z \tag{A3c}$$

Acknowledgments

References

[1]Lefferts, E. J., Markley, F. L., and Shuster, M. D., "Kalman Filtering for Spacecraft Attitude Estimation," *Journal of Guidance, Control, and Dynamics*, Vol. 5, No. 5, 1982, pp. 417–429.

[2]Kudva, P., and Throckmorton, A., "Attitude Determination Studies for the Earth Observation System AM1 (EOS-AM1)Mission," *Journal of Guidance, Control, and Dynamics*, Vol. 19, No. 6, 1996, pp. 1326–1331.

[3]Flatley, T. W., Forden, J. K., Henretty, D. A., Lightsey, E. G., and Markley, F. L., "On-Board Attitude Determination and Control Algorithms for SAMPEX," *Proceedings of Flight Mechanics/Estimation Theory Symposium*, edited by T. Stengle, NASA CP 3102, 1990, pp. 379–398.

[4]Chu, D., Glickman, J., and Harvie, E., "Improvements in ERBS Attitude Determination Without Gyros," edited by T. Stengle, *Proceedings of Flight Mechanics/Estimation Theory Symposium*, NASA CP 3186, 1992, pp. 185–200.

[5]Gai, E., Daly, K., Harrison, J., and Lemos, L.,"Star-Sensor-Based Satellite Attitude/Attitude Rate Estimator," *Journal of Guidance, Control, and Dynamics*, Vol. 8, No. 5, 1985, pp. 560–565.

[6]Psiaki, M. L., Martel, F., and Pal, P. K., "Three-Axis Attitude Determination via Kalman Filtering of Magnetometer Data," *Journal of Guidance, Control, and Dynamics*, Vol. 13, No. 3, 1990, pp. 506–514.

[7]Polites, M. E., and Lightsey, W. D., "A Nonlinear Estimator for Reconstructing the Angular Velocity of a Spacecraft Without Rate Gyros," NASA TP-3178, Dec. 1991.

[8]Challa, M. S., Natanson, G. A., Baker, D. F., and Deutschmann, J. K., "Advantages of Estimating Rate Corrections During Dynamic Propagation of Spacecraft Rates—Applications to Real-Time Attitude Determination of SAMPEX," edited by K. R. Hartman, *Proceedings of Flight Mechanics/Estimation Theory Symposium*, NASA CP 3265, 1994, pp. 481–495.

[9]Challa, M., Kotaru, S., and Natanson, G., "Magnetometer-Only Attitude and Rate Estimates During the Earth Radiation Budget Satellite 1987 Control Anomaly," *Proceedings of the AIAA Guidance, Navigation, and Control Conference*, Vol. 2, AIAA, Reston, VA, 1997, pp. 830–840.

[10]Challa, M., Natanson, G., and Ottenstein, N., "Magnetometer-Only Attitude and Rates For Spinning Spacecraft," *Proceedings of the AIAA/AAS Astrodynamics Specialists Conference*, AIAA, Reston, VA, 2000, pp. 311–321.

[11]Crassidis, J. L., and Markley, F. L., "Predictive Filtering for Attitude Estimation Without Rate Sensors," *Journal of Guidance, Control, and Dynamics*, Vol. 20, No. 3, 1997, pp. 522–527.

[12]Azor, R., Bar-Itzhack, I. Y., and Harman, R. H., "Satellite Angular Rate Estimation from Vector Measurements," *Journal of Guidance, Control, and Dynamics*, Vol. 21, No. 3, 1998, pp. 450–457.

[13]Algrain, M. C., and Saniie, J., "Interlaced Kalman Filtering of 3-D Angular Motion Based on Euler's Nonlinear Equations," *IEEE Transactions on Aerospace and Electronic Systems*, Vol. 30, No. 1, 1994, pp. 175–185.

[14]Harman, R. R., and Bar-Itzhack, I. Y., "Pseudolinear and State-Dependent Riccati Equation Filters for Angular Rate Estimation," *Journal of Guidance, Control, and Dynamics*, Vol. 22, No. 5, 1999, pp. 723–725.

[15]Azor, R., Bar-Itzhack, I. Y., Deutschmann, J. K., and Harman, R. R., "Angular Rate Estimation Using Delayed Quaternion Measurements," *Journal of Guidance, Control, and Dynamics*, Vol. 24, No. 3, 2001, pp. 436–443.

[16]Bar-Itzhack, I. Y., "Classification of Algorithms for Angular Velocity Estimation," *Journal of Guidance, Control, and Dynamics*, Vol. 24, No. 2, 2001, pp. 214–218.

[17]Golub, G. H., and Van Loan, C. F., *Matrix Computations*, 1st ed., Johns Hopkins Univ. Press, Baltimore, MD, 1983, Chap. 2, p. 19.

[18]Markley, F. L., and Mortari, D., "How to Estimate Attitude from Vector Observations," American Astronautical Society, AAS Paper 99-427, Aug. 1999.

[19]Shuster, M. D., "Maximum Likelihood Estimation of Spacecraft Attitude," *Journal of the Astronautical Sciences*, Vol. 37, No. 1, 1989, pp. 79–88.

[20]Markley, F. L., "Attitude Determination Using Vector Observations and the Singular Value Decomposition," *Journal of the Astronautical Sciences*, Vol. 36, No. 3, 1988, pp. 245–258.

[21]Psiaki, M. L., Theiler, J., Bloch, J., Ryan, S., Dill, R. W., and Warner, R. E., "ALEXIS Spacecraft Attitude Reconstruction with Thermal/Flexible Motions Due to Launch Damage," *Journal of Guidance, Control, and Dynamics*, Vol. 20, No. 5, 1997, pp. 1033–1041.

[22]Psiaki, M. L., and Oshman, Y., "Spacecraft Attitude Rate Estimation from Geomagnetic Field Measurements," AIAA Paper 2002-4828, Aug. 2002.

[23]Tortora, P., Oshman, Y., and Santoni, F., "Spacecraft Angular Rate Estimation from Magnetometer Data Only Using an Analytic Solution of Euler's Equations," Dept. of Aerospace Engineering, Technion—Israel Inst. of Technology, TR TAE-909, Haifa, Israel, Dec. 2002.

C. A. Kluever
Associate Editor